

## Photon mean free paths, scattering, and ever-increasing telescope resolution

P.G. Judge<sup>1</sup> · L. Kleint<sup>2</sup> · H. Uitenbroek<sup>3</sup> ·  
M. Rempel<sup>1</sup> · Y. Suematsu<sup>4</sup> · S. Tsuneta<sup>4</sup> ·

© Springer ....

**Abstract** We revisit an old question: what are the effects of observing stratified atmospheres on scales below a photon mean free path  $\lambda$ ? The mean free path of photons *emerging* from the solar photosphere and chromosphere is  $\approx 10^2$  km. Using current 1m-class telescopes,  $\lambda$  is on the order of the angular resolution. But the Daniel K. Inoue Solar Telescope will have a diffraction limit of  $0.020''$  near the atmospheric cutoff at 310nm, corresponding to 14 km at the solar surface. Even a small amount of scattering in the source function leads to physical smearing due to this solar “fog”, with effects similar to a degradation of the telescope PSF. We discuss a unified picture that depends simply on the nature and amount of scattering in the source function. Scalings are derived from which the scattering in the solar atmosphere can be transcribed into an effective Strehl ratio, a quantity useful to observers. Observations in both permitted (*e.g.*, Fe I 630.2 nm) and forbidden (Fe I 525.0 nm) lines will shed light on both instrumental performance as well as on small-scale structures in the solar atmosphere.

**Keywords:**

### 1. Introduction

The photosphere and lower chromosphere are hydrostatically stratified atmospheric layers of the Sun from which the bulk of the solar radiation emerges. In this paper we study the effects of observing these regions on scales below  $\lambda$ , the

---

<sup>1</sup> High Altitude Observatory, National Center for Atmospheric Research<sup>5</sup>, email: judge@ucar.edu, rempel@ucar.edu

<sup>2</sup> Institute of 4D Technologies, University of Applied Sciences and Arts Northwestern Switzerland, 5210 Windisch, Switzerland lucia.kleint@fnhw.ch

<sup>3</sup> National Solar Observatory, email: huitenbroek@nso.edu

<sup>4</sup> National Astronomical Observatory of Japan, email: suematsu@solar.mtk.nao.ac.jp, saku.tsuneta@nao.ac.jp

<sup>5</sup> The National Center for Atmospheric Research is sponsored by the National Science Foundation

**Table 1.** Spectral lines commonly used to determine thermal and magnetic structure

$\lambda$ nm	log gf	Ion	Lower level	Upper level	$z$ km	$-\log_{10} \epsilon$
422.6728	+0.243	Ca I	$4s^2 \ ^1S_0$	$4s4p \ ^1P_1^o$	200-1000 <sup>a</sup>	2.9-4.5 <sup>h</sup>
524.7049	-4.946	Fe I	$a \ ^5D_2$	$z \ ^7D_3^o$	0-500 <sup>b</sup>	0-0.01
525.0208	-4.938	Fe I	$a \ ^5D_0$	$z \ ^7D_1^o$	0-500 <sup>b</sup>	0-0.02
589.5924	-0.184	Na I	$3s \ ^2S_{1/2}$	$3p \ ^2P_{1/2}^o$	50-700 <sup>c</sup>	1.4-3.7
617.3341	-2.880	Fe I	$a \ ^5P_1$	$y \ ^5D_0^o$	20-300 <sup>d</sup>	1.0-2.3
630.1498	-0.745	Fe I	$z \ ^5P_2^o$	$e \ ^5D_2$	20-210 <sup>e</sup>	0.9-1.9
630.2494	-1.203	Fe I	$z \ ^5P_1^o$	$e \ ^5D_0$	20-210 <sup>e</sup>	0.9-1.9
676.7768	-2.170	Ni I	$a \ ^1S_0$	$z \ ^3P_1^o$	250-450 <sup>f</sup>	0.5-1.0
709.0378	-1.210	Fe I	$y \ ^5D_1^o$	$e \ ^5F_1$	200-500 <sup>a</sup>	1.7-2.8
854.2091	-0.362	Ca II	$3d \ ^2D_{5/2}$	$4p \ ^2P_{3/2}^o$	200-1300 <sup>g</sup>	0.8-2.6

Notes: Oscillator strengths are from 1995 Atomic Line Data (R.L. Kurucz and B. Bell) Kurucz CD-ROM No. 23. Cambridge, Mass.: Smithsonian Astrophysical Observatory. Values of  $\epsilon$  are computed for the range of formation heights listed, using the Van Regemorter approximation for permitted transitions. For the spin forbidden transitions a cross section of  $\pi a_0^2$  was used where  $a_0$  is the Bohr radius. Formation heights are from: *a* from VAL model 3C, computed in this work; *b* 525.0 from Lites (1973), with 325 km added (the limb-to-center viewing angle correction, *e.g.* Athay (1976)), 524.7 assumed the same; *c* Leenaarts *et al.* (2010); *d* Norton *et al.* (2006); *e* Faurobert, Ricort, and Aime (2013); *f* Bruls (1993); *g* Cauzzi *et al.* (2008). *h* A collision strength of 14.4 was adopted here instead of the Van Regemorter approximation.

mean free path (mfp) of photons. Our goals are to explain some physical effects resulting from photon scattering, to examine basic limitations that the Sun itself presents, and to quantify their dependence on the nature of the scattering. On scales currently observable with 1m class telescopes near 500nm,  $\lambda$  is on the order of the angular resolution. But the 4m Daniel K. Inoue Solar Telescope will have a diffraction limit of 0.020'' near 310nm, 0.038'' near 600nm, corresponding to 14 and 27 km at the solar surface. These are mere fractions of  $\lambda$ .

In the Sun's atmosphere, magnetoconvection and other processes can generate thermal and magnetic structure on scales significantly below  $\lambda$ . This is because local radiative losses and gains do not necessarily occur over spatial scales dictated by the continuum mean free path. The gains/losses arise from integrals over the whole spectrum, including many lines far more opaque than the neighboring continuum, with far smaller photon mfps. MHD processes create structures with non-zero temperature contrast on spatial scales much smaller than the continuum mean free path (*e.g.* Knoelker, Schuessler, and Weisshaar, 1988). We do not address this problem here. Instead we examine limitations imposed by photon scattering.

Many authors have explored this problem using spectral lines with diverse scattering properties. We will show that the various calculations in the literature are readily understood taking into consideration the "scattering parameter"  $\epsilon$ . Defined below (equation 1), this measures the probability of photon destruction per interaction with the atom. A list of spectral lines commonly used to explore the Sun's magnetic and thermal atmospheric structure is given in Table 1. Note that they too have a variety of scattering parameters.

“Spatial resolution” is a problem not only in the usual, “plane-of-the-sky” sense, but also along the line-of sight (LOS) direction. This is of physical interest, because measurements of LOS derivatives in the magnetic field vector  $\mathbf{B}$ , in particular, are important for physical and technical reasons (e.g. Socas-Navarro, 2005). The ability of a telescope/spectrograph to resolve features along the LOS has been discussed by Landi degl’Innocenti (2013). Within a stratified atmosphere the thickness of the spectrum-forming layer – that from which the photons last interact with the matter – is always roughly a local pressure scale height. We show this formally in Appendix A, and review why the intensity regulated by the  $H^-$  ion, which dominates the visible continuum opacity, forms naturally over half the distance. To look at the ability of telescopes to resolve features in the POS, below we examine radiative transfer calculations including varying amounts of photon scattering. To understand the calculations we use equations for the source function  $S$  of the form

$$S = (1 - \epsilon)J + \epsilon B. \quad (1)$$

Here  $B$  is the Planck function and the meanings of  $\epsilon$  and mean intensity  $J$  are different for coherent scattering and for incoherent scattering in spectral lines (see below).

The development of efficient transfer algorithms in the 1980s (e.g. Scharmer and Carlsson, 1985; Rybicki and Hummer, 1991) has made multi-dimensional transfer calculations more common, particularly using algorithms making use of local coupling between radiation and matter. But the literature has tended to focus on dynamical simulations and/or effects on Stokes profiles (e.g. Kiselman and Nordlund, 1995; Leenaarts *et al.*, 2010; Leenaarts, Carlsson, and Rouppe van der Voort, 2012; Holzreuter and Solanki, 2012, 2013). We focus instead on the non- local thermodynamic equilibrium (nLTE) intensity problem alone, emphasizing the understanding of previous work and offering suggestions for spectral line observations with new large telescopes. In Section 2 we review earlier work addressing effects on solar images, i.e. effects of scattering in the POS. Section 3 presents radiative transfer calculations and derives scalings of properties of the emergent intensity on the nature of the scattering and on atomic parameters. Section 4 combines the results and explains some observations of very fine structures seen against the solar disk (filaments, spicules). In Appendix B we remind readers that the bulk of the chromosphere is close to a hydrostatic stratification and therefore subject to the main arguments in this paper. (Dynamic phenomena such as spicules have attracted much recent attention, but these must arise from far more tenuous structures, merely being at chromospheric temperatures).

## 2. Earlier work

Avrett and Loeser (1971) presented two component nLTE calculations in regimes close to solar. They solved for source functions at two points inside and between thermally different hexagonal columns in static but stratified layers, for a 2-level

atomic model of the chromospheric Ca II K line. Being a two level calculation the problem is linear (source function is linear in intensity):

$$S_L = (1 - \epsilon)\bar{J} + \epsilon B. \quad (2)$$

where  $\bar{J} = \int J_\nu \phi_\nu d\nu$  is the mean intensity weighted across the line profile  $\phi_\nu$  and  $\int \phi_\nu d\nu = 1$ , see Mihalas (1978). They assumed complete redistribution (CRD) in the scattering terms in the source functions. They adopted realistically small but fixed values of  $2 \times 10^{-4}$  for the photon scattering parameter, which we define as the destruction probability:

$$\epsilon = \mathcal{C}_{ji}/(\mathcal{C}_{ji} + A_{ji}), \quad (3)$$

where  $\mathcal{C}_{ji}$  ( $\text{s}^{-1}$ ) is the transition probability between upper level  $j$  and lower level  $i$  induced by collisions, and  $A_{ji}$  is the spontaneous radiative transition probability.<sup>1</sup> Horizontal transport of radiation showed two essential effects. Firstly, for a homogeneous opacity scale but with the Planck function differing by a factor between 2 and 3 between the components, horizontal variations in intensity become significantly reduced (factor 2 or so) when temperature inhomogeneities are smaller than about four times the opacity scale height, occurring mostly in the centrally reversed portions of the line profile (line center optical depths below 100 or so). Secondly, for a horizontally homogeneous Planck function but with opacities differing by factors of four, the 2D transfer effects cause significant deviations in emergent intensity extending far deeper (line center optical depths of  $10^{3-4}$ ).

Stenholm and Stenflo (1977, 1978) made 2D nLTE transfer calculations in flux tube atmospheres, the latter paper including Zeeman-induced polarization. However, they used the spin-changing transition of Fe I at 525 nm which, with an oscillator strength near  $10^{-5}$  has  $\epsilon$  close to 1, minimizing effects of scattering when compared with permitted transitions (see Table 1).

Kneer (1981) reviewed 2D radiative transfer calculations in stratified atmospheres, pointing to some that appeared to contradict each other. Kneer (1981) therefore made nLTE linear transfer calculations using two limits- pure coherent scattering (CS) whose diffusive behavior mimics the partially CS regime applicable to the wings of strong lines - and complete redistribution for a 2 level atom. He studied harmonic variations in the Planck function in a stratified atmosphere with opacity a function of height, for fixed values of  $\epsilon$  between  $10^{-6}$  to  $10^{-1}$ . His results confirmed that lateral transfer, especially in the chromosphere, decreases the contrast in images as nLTE effects increase (decreasing  $\epsilon$ ), even on scales above the resolution of telescopes then available. Kneer introduced the modulation transfer function (MTF) of the calculated intensities which is readily combined with the point spread functions of telescopes, to arrive at a quantitative way to study the relative smearing of solar thermal structure by solar effects (scattering) and by the observing instrument. Kneer confirmed and

---

<sup>1</sup>Since in this paper we focus on visible and infrared wavelengths we ignore photon destruction by continuous absorption which dominates at UV and mm/radio wavelengths.

extended to CRD cases random walk arguments of Owocki and Auer (1980) in which the length scales of lateral transport, defined through the PSF full width at half maximum, vary as

$$\ell \approx a + \ln \tau_{th}. \quad (4)$$

Here,  $a \approx 1$  and  $\tau_{th}$ , the thermalization length measured in units of monochromatic or line center optical depth, varies asymptotically as  $\approx \epsilon^{-1/2}$  (CS) or  $\approx \epsilon^{-1}$  (CRD). The different powers of  $\epsilon$  arise because CRD over-estimates the production of wing photons from the core, enhancing photon escape over the CS approximation (see *e.g.* Mihalas, 1978). In effect, Kneer provided a unified picture of various calculations available in 1980.

The problem was revisited by Bruls and Von der L  he (2001). Their goal was to show that it is possible to resolve structures on scales significantly *below*  $\lambda$ , in the POS. As a measure of “resolution” they simply looked for visible structure in emergent intensities around two magnetic flux sheets, without discussing MTFs or PSFs. Their calculations of the spin forbidden lines of Fe I (524.7 and 525.0 nm) and the Ca II line intensities presents however a mixed set of conditions. On the one hand they emphasize the nLTE process of photoionization in which iron is over-ionized by UV radiation. In essence, all the nLTE for the iron calculation is in the line opacities but not, for these spin forbiddent lines, the source function. For the permitted and strong calcium lines, the very opposite is true, and for these lines their work appears consistent with the earlier work of, for instance, Avrett & Loeser and Owocki & Auer.

Below we will study in isolation one source of “nLTE” conditions- the scattering parameter, and we will relate the calculations and their parameters to an “effective PSF” as seen with a perfect, diffraction-free telescope. Over-ionization of elements by transfer of UV radiation is arguably less important as a smearing agent than scattering in spectral lines observable from the ground, because UV opacities are orders of magnitude higher than at visible wavelengths, with correspondingly smaller values of  $\lambda$ .

### 3. Telescope resolution vs. spectrum formation

#### 3.1. Isolated thermal sources: line of sight averaging

All spectra are formed over finite depths in a stratified atmosphere. Appendix A shows why this depth is an opacity scale height, equal to a density scale height  $H$  for most atomic transitions and 1/2 of this for the  $H^-$  ion. Let  $\Delta \approx H$  describe the *width* of the distribution of heights from which the photons emerge along a given line of sight. The centroid of this distribution can be determined far more accurately- all that is required is that we have enough photons  $N$  in our measurement to make photon noise variations  $\approx \sqrt{N}$  much smaller than  $N$  itself. Imagine for simplicity isolated bright point thermal sources of emission, with

$$S = B \quad (5)$$

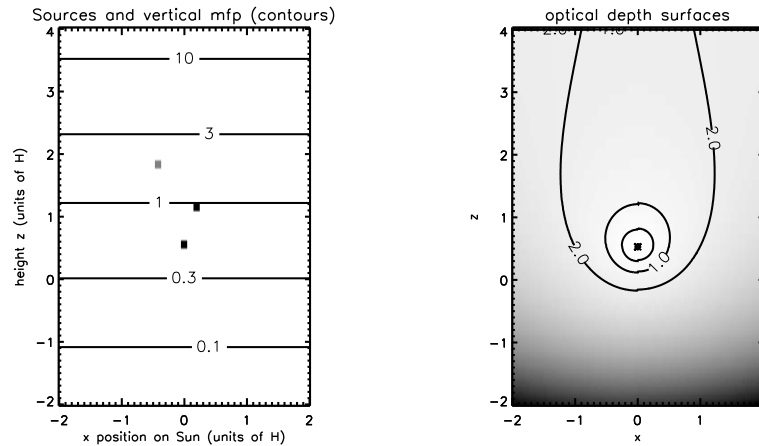


**Figure 1.** Left: Isolated sources of radiation embedded in a stratified, scattering atmosphere are shown. No thermal sources of emission other than the three bright points shown were included. Contours show the local mean free path length. All distances are in units of the local density scale height  $H$ . The two sources are placed just below the  $\tau = 1$  surface (contour of mfp = 1) and are separated by  $1/2$  of a pressure scale height. Right: surfaces of constant optical depth are shown as an image (reverse colors, dark=larger values) and with contours, calculated from the deepest of the sources shown in the left hand panel. The  $\tau = 1$  surface is egg-shaped. Radiation escapes preferentially in the outward (positive  $z$ ) direction.

in a stratified atmosphere that can also absorb photons (scattering is dealt with below). The configuration is shown in Figure 1.

If we could observe from several angles (*i.e.* stereoscopically) we would be able to determine the mean formation heights to within measurement errors provided that we capture enough photons. *But* from just one line of sight, the sources have an intrinsic uncertainty in their position of origin of about  $\lambda \approx H \approx 10^2$  km (Landi Degl’Innocenti, 2013).

The condition that we have a large number  $N$  of photons is nothing more than saying that the standard deterministic transfer equation can be applied. At the resolution limit of telescopes, with a Planck function near 6000K, a spectral resolution of  $10\text{m}\text{\AA}$ ,  $N \approx 2 \times 10^7 t E$ , where  $t$  is the integration time in s, and  $E < 1$  is the transmission efficiency of the optical system. There are plenty of photons for reasonable values of  $t$  and  $E$ . Thus the *relative* centroids of the “heights of formation” of various lines can be determined to most desired levels of accuracy, but their absolute (heliocentric) coordinates have an intrinsic uncertainty of around  $H$ . The measurement becomes photon starved when trying to measure weak polarization signals (Landi Degl’Innocenti, 2013).

### 3.2. Isolated thermal sources: plane of sky smearing

In the plane of the sky, strict thermal sources can be resolved down to a telescope resolution scale. This is because along each line of sight, the source functions are purely local and independent of neighboring lines of sight. A feature in the atmosphere is either intercepted by a ray or it is not. For pure thermal emission

two sources separated by  $< \lambda$  can be resolved. The same is true for isolated optically thin sources in the corona (see the Discussion).

Returning to stratified atmospheres, it must be kept in mind that there is always a line of sight integration of scale length  $\Delta \approx H$ , so any fine scale source structure along a length  $H$  (such as associated with current sheets surrounding magnetic flux concentrations) is averaged along the LOS.

### 3.3. Isolated sources including coherent scattering

Consider the more general case where the sources include coherently scattered photons

$$S_\nu = \epsilon B_\nu + (1 - \epsilon)J_\nu, \quad (6)$$

where the probability of photon destruction is  $\epsilon = \frac{\kappa_a}{\kappa_a + \kappa_s}$ , and  $\kappa_a$  and  $\kappa_s$  are the opacities for pure absorption and scattering respectively (the total opacity being  $\kappa = \kappa_a + \kappa_s$ ). The quantity  $\eta = 1 - \epsilon$  is the scattering albedo, and  $J_\nu$  is the angle-averaged intensity at frequency  $\nu$ . Now the formal solution to the transfer equation is written operationally as

$$J_\nu = \Lambda[S_\nu] \quad (7)$$

where  $\Lambda$  is an integral operator over all space. The source function (equation 6) is now *non-local*, requiring one to solve a familiar integro-differential equation. For simplicity, first consider a 1D stratified atmosphere. The range of  $\Lambda$  as measured in photon mean free paths is the “thermalization length”  $\tau_{th}$ : in essence all regions of the atmosphere that lie within  $\tau_{th}$  mean free paths of a given point influence the value of  $J_\nu$  and hence  $S_\nu$  there. Given that the vertical emergent intensity  $\approx S_\nu(\tau = 1)$ , we must therefore be aware that equation (7) represents a *physical smearing* of the original thermal source of photons  $\epsilon B_\nu$ .

As already noted, the value of  $\tau_{th}$  in 1D atmospheres scales with  $\epsilon$  as (Mihalas, 1978)

$$\tau_{th} \approx 1/\sqrt{\epsilon} \quad (\text{coherent scattering}), \text{ and } \approx 1/\epsilon \quad (\text{spectral lines}) \quad (8)$$

where coherent scattering occurs only by diffusion in space and lines scatter by diffusion in space and redistribution in frequency. Wings of strong spectral lines form under conditions close to CS, the cores more like CRD - the  $1/\epsilon$  factor applies to typical cases where “partial redistribution” is important (Mihalas, 1978). The dependence of  $\tau_{th}$  on  $\epsilon$  is stronger for permitted line transitions instead of strict CS as photons are redistributed in frequency as well as space. As a consequence, for lines, one must consider the frequency averaged mean intensity  $\bar{J}$  not just  $J_\nu$ . For strong scattering ( $\epsilon \ll 1$ ), the  $\Lambda$  operator smears the source function over a large number of mfps. In the case of strong chromospheric lines (Ca II and Mg II resonance lines, for example), the thermalization depth spans most of the 1500 km thickness of the stratified chromosphere (*e.g.* Linsky and Ayres, 1978). In weaker lines formed in the photosphere, such as spin forbidden transitions (*e.g.* Fe I 524.7 and 525.0 nm),  $\epsilon$  is close to unity and the source function returns to LTE.

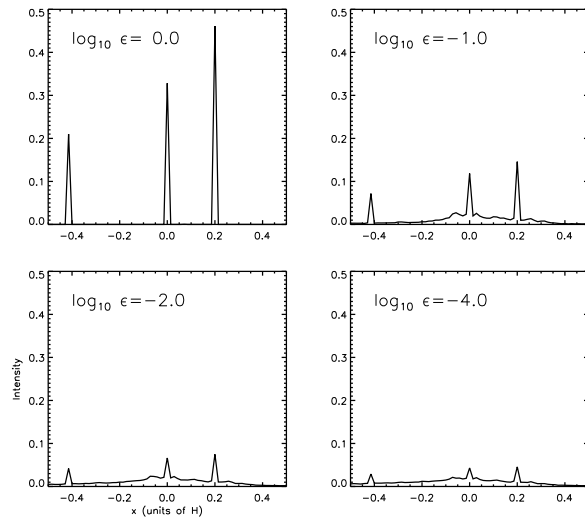


**Figure 2.** Emergent intensity as a function of  $x$  as seen from an inclination of zero. The integrals under the curves are the same.

In 3D the microphysics is the same, but we must imagine instead a ‘thermalization volume’ around a given point which contains all sources that can influence the source function at that particular point. For a 3D stratified atmosphere this volume will look on average like a distorted egg with a squashed bottom and a stretched or open top (Figure 1). The radiative transport becomes 1D-like because lateral transport effects, in particular through the  $\Lambda$  operator, are less efficient than vertical escape of radiation.

Figure 2 shows results of a Monte Carlo calculation of the emergent intensity from the thermal sources shown in Figure 1 for different values of the destruction probability  $\epsilon$ , assuming CS. The calculation has been set up to make any scattering effects important, by placing the sources both beneath and above the optical depth unity surface. (If deeper, the mfps would be very small, if higher, the mfps would be very large and the radiation optically thin).

Differences between these calculations simply reflect the scattering process *in the Sun itself*. Sub-mfp scales can be resolved, but enhanced scattering in the Sun produces a diffuse image that appears qualitatively like a telescope that has broad wings in the PSF (see Fig. 2), at least for features formed below the vertical  $\tau = 1$  surface. The smoothing is on scales smaller than  $\lambda \approx H$  in part because the outward directed photons tend to escape and be observed with fewer scatterings than inward or horizontally directed photons. Therefore, the lateral effects of scattering are smaller than in non-stratified cases. This is a well known result used in early days to justify calculations with transport only in the vertical (radial) direction. In Section 4.1 we discuss some scalings arising from these calculations.

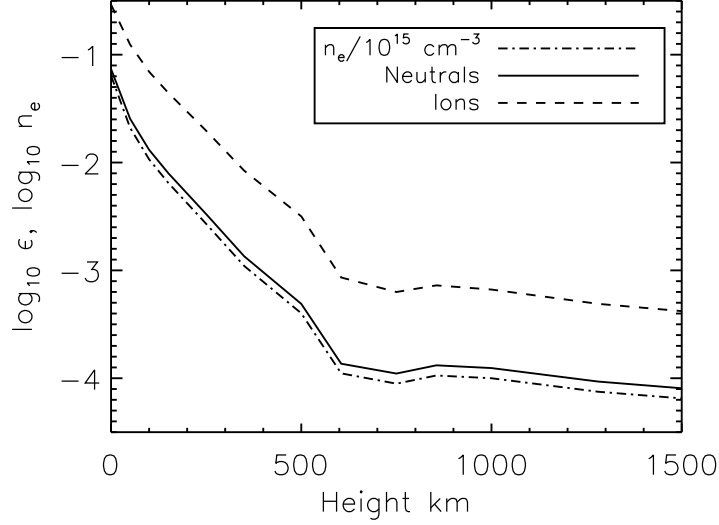


**Figure 3.** Destruction probabilities are shown as a function of height for the model 'C' atmosphere of Vernazza, Avrett, and Loeser (1981), for permitted transitions, using Van Regemorter's (1962) approximation. A wavelength of 500 nm was used to make this plot.

#### 3.4. Line transfer scalings

The lines listed in Table 1 are all electric dipole transitions of abundant elements. To estimate scattering parameters for those fully permitted lines (i.e. excluding spin-forbidden lines of 524.7, 525.0 and 676.8 nm), we adopt the estimate of Van Regemorter (1962), in which the long-range interaction between the incoming electrons and the atom dominates the cross section, and produces collision probabilities that are proportional to the radiative transition probability. Van Regemorter's formula is

$$C_{ji} = 20.60 \lambda^3 T_e^{-1/2} p_z (hc/\lambda kT) A_{ji} \quad (9)$$

where  $\lambda$  is in cm,  $T_e$  in K, and  $p_z(\beta)$  are weakly decreasing functions of  $\beta$  for ions (charge  $z \geq 1$ ), and another that varies asymptotically as  $\beta^{-1/2}$  for large  $\beta$  in neutrals ( $z = 0$ ). The Maxwellian-averaged transition probability for collisional de-excitation by electrons of number density  $n_e$  between the atomic levels  $i$  and  $j$  is  $C_{ji} = n_e C_{ji} \text{ s}^{-1}$ , and the spontaneous radiative emission coefficient is  $A_{ji} \text{ s}^{-1}$ . Van Regemorter's equation (22) gives

$$\epsilon' = \frac{n_e C_{ji}}{A_{ji}} = 20.60 n_e \lambda^3 T_e^{-1/2} p_z (hc/\lambda kT), \quad (10)$$

for the ratio of collision de-excitation rates by electrons of number density  $n_e$  to  $A_{ji}$ .  $\epsilon'$  depends only weakly on  $T_e$  which in any case changes far less than the electron density across the solar photosphere/chromosphere. The destruction

probability is

$$\epsilon = \frac{n_e C_{ji}}{n_e C_{ji} + A_{ji}} = \frac{\epsilon'}{1 + \epsilon'}. \quad (11)$$

Estimates of  $\epsilon$  for the Sun’s atmosphere are shown in Figure 3, using the stratified model ‘C’ of Vernazza, Avrett, and Loeser (1981). Lines of neutrals differ from those of charged ions because of the different behavior of cross sections at threshold (Seaton, 1962). For the transitions involving changes of spin– 524.7, 525.0 and 676.8 nm– we assumed cross sections of  $\pi a_0^2$  with  $a_0$  the Bohr radius, since such transitions require penetration of the target atom by the electron (long range dipole interactions are small). The  $\epsilon$  values are probably no better than order of magnitude estimates given the approximations involved (Allen, 1973). Since collisions with other particles and to other atomic levels, and background continuum absorption are not included, they are probably under-estimates by factors between one and two.

Values of  $\epsilon$  listed in Table 1 vary between one (spin-forbidden transitions) to  $10^{-4.5}$  (strong lines with contributions to their formation above heights of 500 km). From these calculations we see that, in order to minimize the kind of scattering effects shown in Figure 2, the spin-forbidden lines with  $\epsilon$  parameters close to unity should be used. Indeed, differences between these the stronger permitted lines with far smaller values of  $\epsilon$  should be exploited in observational campaigns with high resolution telescopes.

### 3.5. 3D Line transfer calculations in magnetoconvection simulations

We have made calculations using the 422.7 nm line of Ca I using the 3D nLTE radiative transfer program “RH” of Uitenbroek (2000), in magnetoconvection models generated by using the MURaM code by one of us (Rempel, 2014). These are small scale dynamo models (*i.e.* a mixed polarity field is maintained self-consistently by turbulent flows) in a  $6.144 \times 6.144 \times 3.072 \text{ Mm}^3$  domain with a grid spacing of 8 km. The radiation field is treated using a gray opacity, assuming LTE. The average  $\tau = 1$  surface is located about 700 km beneath the top boundary. These models include all thermal structure and vector velocity and magnetic fields, but we have here simply looked at the effects of radiation transport ignoring magnetic and velocity fields, keeping only the 3D thermal structure, for simplicity. Both magnetic and velocity fields distribute opacity over broader wavelength ranges, thereby enhancing radiative transport. Our calculations can be regarded as minimizing the multi-dimensional transfer effects.

Ca I was selected since it is a resonance line formed both in the photosphere and lower chromosphere. We made some trade-offs with regard to the atomic model used for our computations. The calculations are CPU intensive using a large atomic model, and so we included just the two levels of the Ca I 422.7 nm (resonance) line and the Ca II continuum state. Another trade-off was the use of a factor of 3 reduction in abundance (we used 5.86 on a scale where  $H \equiv 12$ ), in order to reduce the optical depth at the very top of the simulations. Our calculations are therefore not to be taken as “synthetic Ca I” data but as

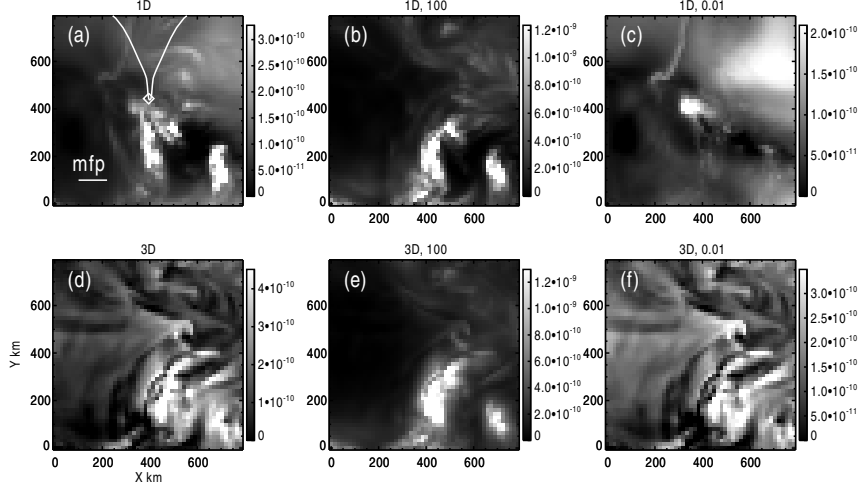


**Figure 4.** Images in the core of the Ca I resonance line computed from a 3D magnetoconvection model. The top row shows intensities computed from 1D transfer calculations along the vertical for each individual pixel. The left panel also shows the wavelength marked with a diamond symbol plotted over the mean line profile. The second row shows the full 3D calculations. From left to right, the values of  $\epsilon$  used were 1, 100 and 0.01 respectively. The images correspond to about  $1 \times 1$  seconds of arc, as observed from Earth, and the “pixels” are 16 km or about  $1/45$  of an arcsecond.

numerical experiments designed to examine the effects of the diffusion of photons in space and frequency for conditions of interest in the Sun’s atmosphere.

Figure 4 compares the results from 1D and 3D calculations for several different values of the parameter  $\epsilon$ , at the center of the Ca I line. The nominal value of  $\epsilon$  uses the collision rates in the atomic model included with RH- it amounts to a cross section about  $3\times$  larger than the Van Regemorter formula would give. Values of  $\epsilon$  were changed simply by multiplying the collision rates between the two singlet levels by factors of  $10^2$  and  $10^{-2}$ .

Panels (b) and (e) have the closest 1D vs. 3D properties, as expected since the line is formed closest to LTE in both cases. Nevertheless, the 3D images are still blurry compared with 1D. Notice that the lines are a factor of 3-4 brighter than the other four calculations that are farther from LTE. Panels (a) and (d) show remarkable qualitative differences attributable to horizontal transfer, indeed on these scales one might wonder if one were looking at the same region of the Sun. (c) and (f), furthest from LTE, are also radically different, with the  $\epsilon = 0.01$  3D case being some 30% dimmer than, with less contrast than the 3D case for  $\epsilon = 1$ .

The differences in images generated at different wavelengths (not shown) are progressively smaller as wavelengths move from the core to the wings. This is expected since the line opacity is relatively smaller and the LTE continuum, dominated by  $H^-$  absorption, making significant contributions to both source

function and optical depth. Images made in 3D at 0.01 nm to the blue of line center are similar in overall appearance to panel (c), panel (c) therefore shows structure a little deeper in the atmosphere compared with the others shown. At these inner wing wavelengths, qualitatively similar effects are seen as in the line core in terms of blurring, but the images are more similar to one another.

The images all show structure below the vertical photon mfp. However, the image contrasts are reduced compared with 1D calculations owing to horizontal radiative transfer and they can even have a very different morphology. The former results are consistent with the narrative by Kneer (1981). The effects of scattering cannot therefore automatically be neglected, except perhaps for the continua ( $H^-$ ) and weak photospheric lines formed strictly in LTE. They become more important as stronger features form successively higher in the atmosphere as the densities decrease with height. Leenaarts *et al.* (2010) indeed report “halos” around features in the very low  $\epsilon$  Na I D lines in their radiation MHD calculations.

## 4. Discussion

### 4.1. nLTE transfer can mimic a poor telescope PSF

The scattering intrinsic to solar plasma has a similar effect to reducing the imaging performance of a telescope. This was explored by Kneer (1981) in terms of a modulation transfer function  $M_I(k)$  (MTF):

$$M_I(k) = I'(k)/I'(k=0) \quad (12)$$

where the Planck function is assumed to vary horizontally harmonically as  $a + b \cos kx$  ( $x$ =horizontal direction),  $I' = I - \langle I \rangle$ ,  $I$  the output intensity and  $\langle I \rangle$  the horizontally averaged output intensity. His figures 2 and 5 compare the MTFs of CS and CRD calculations with a 1m telescope MTF, showing the dramatic drop of the MTFs with decreasing  $\epsilon$  and increasing  $k$  values, and the smaller MTFs for CRD versus CS. The Hankel transform of the MTF gives the point spread function (PSF) of the scattering atmosphere. His figures 3 and 6 compare the computed PSFs using values of  $\epsilon$  from  $10^{-6}$  to  $10^{-1}$ , with telescope PSFs for various length scales  $k^{-1}$ . The figures show the detrimental effects of the scattering clearly broadens the PSF as  $\epsilon$  decreases. Also, his Figure 7 shows the computed full width at half maximum (FWHM) of the PSFs as functions of  $\tau_{th}$  which have the dependence of equation 4.

For our purposes we use the simple definition of the Strehl ratio as the ratio of the peak image intensity from a point source to the maximum attainable intensity using an ideal optical system. We then estimate for each synthetic calculation (independent of any telescope system) an equivalent Strehl ratio. We use intensities along vertical rays.

Figure 6 shows that the equivalent Strehl ratio  $\mathcal{S}$  for CS for the embedded sources used varies for large  $\epsilon$  as

$$\mathcal{S} \approx \sqrt{\epsilon}, \quad \text{for } \epsilon > 0.1$$

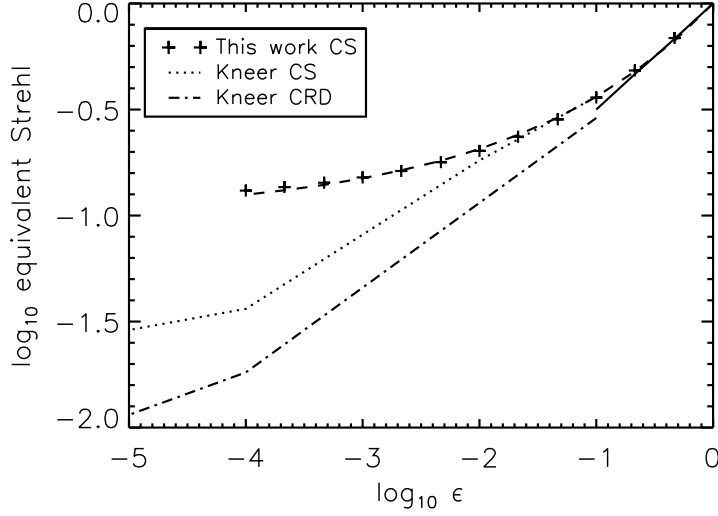


**Figure 5.** The peak brightness, normalized to the case of no scattering ( $\epsilon = 1$ ) taken from the coherent scattering calculation data shown in Figure 2. The ordinate is one useful definition of the equivalent Strehl ratio. The short solid line is  $S = \sqrt{\epsilon}$ , the dashed line  $\log_{10} S = \epsilon^{0.26} - 1$ .

For smaller values of  $\epsilon$ ,  $S$  is weakly dependent on  $\epsilon$ , being  $> 0.1$  for all solar lines of interest. Figure 2 shows that core intensity is moved laterally by up to 1 (vertical) mfp from its thermal source for almost all values of  $\epsilon$ . Taken together, we see that sub $\lambda$  scale, high contrast sources should be distinguishable even in the presence of scattering. Kneer's Figures 4 and 7 in fact already exhibit a similar result (although Kneer himself does not report this). In his case, the central values of the PSFs shown seem to scale with  $\epsilon^\alpha$  with  $\alpha \approx 0.3 - 0.4$ , as shown in our Figure 6. (Kneer does not show results for  $\epsilon = 1$ , therefore we have moved his two curves upwards by 0.2 dex so that his CS calculations agree with ours at  $\epsilon = 0.1$ ). The differences between the calculations are real. We would not expect the curves to agree - these are very different calculations (Kneer has periodic sources spread through his domain, we have point sources at special places near optical depth unity). But the trends are clear, the Strehl ratio decreases initially like  $\epsilon^\alpha$  before beginning to flatten at very small  $\epsilon$  values. We believe flattening arises from stratification which, no matter the number of scatterings, tends to promote photon escape vertically out of the atmosphere.

#### 4.2. A simple conceptual picture

With future telescopes we will routinely observe the Sun's atmosphere at scales  $\ll \lambda$ . In our 2D calculations we have considered isolated bright points separated by length scales  $\delta < \lambda$ . When we have a thermal source function, even when  $\delta \gg \lambda$  the two structures are fully resolved since either the rays intercept the hot structure or they do not, and we assume the source function is negligible outside of the two points. Even if the source function outside is finite, points will

be resolved if their brightness is sufficient to discriminate them from each other and the background. The resolution along one single line of sight remains about one pressure scale height without stereoscopy (Landi Degl’Innocenti, 2013).

The situation is different in the presence of scattering, since the hot source function “leaks” into neighboring regions of the atmosphere with, in 1D, a characteristic length scale for thermalization of  $\lambda/\epsilon^\alpha$ . Our 2D CS calculations suggest that the horizontal scattering should spread the light finally emerging from point sources by about 1 vertical mfp from their origin, and that their “equivalent Strehl ratio” should be around  $\epsilon^\alpha$ ,  $\alpha = 1/3$  to  $1/2$ . Using Kneer’s earlier results the Strehl ratio would be, for CRD in lines, about  $\epsilon^{0.44}$ .

In 3D the situation is more complex and we can estimate that the characteristic length will be some number  $x$  times  $\lambda$ ,  $x \gtrsim 1$ . If  $\delta \lesssim x\lambda$  then some loss of resolution will result. Depending on the 3D thermal structure and scattering parameters though, it may still be possible to resolve the two bright sources, like being able to see two car headlights through a dense fog. Our 3D calculations for a simple Ca I atom support these conclusions. The resolution along one single line of sight in this case is reduced to  $\lambda/\epsilon^\alpha$ , but since the mfps exponentially decrease with depth, this means the LOS resolution may not be that dissimilar from the thermal case.

#### 4.3. Some outstanding questions

There are cases that might appear to contradict the above discussion. These cases seem to require decoupling of optical depth scale from the source function in the optically thin parts of an atmosphere, allowing some fine structures to be imprinted as absorption (or emission) features on a smoother, spatially smeared scattering source function.

Consider the observation of a terrestrial cloud passing between the Sun and telescope. We can resolve the cloud structure down to the telescope’s resolution limit, without regard to the intensity  $I_\odot$  of the background illuminating source (the Sun). In this case the source function in the cloud is negligible, the cloud’s signature is made clear in the image only through the term

$$I = I_\odot e^{-\tau_{cloud}}$$

Thus the measured intensity can have any scale the telescope can resolve along different lines of sight, independent of  $I_\odot$ .

Next imagine an an optically thin “cloud” (spicule, filament, fibril) above the Sun’s photosphere. We might expect the above terrestrial argument to hold. But it must be remembered that close to the Sun there is a low temperature limit to plasma sitting above the solar surface. In the absence of strong adiabatic cooling due to dynamics, the source function at these heights can approach the radiative equilibrium temperature which, for an atmosphere with gray opacity, is near 4000K. The above equation must include this emission. Let the optical depth of a “spicule” be  $\tau_s < 1$  so that with  $I_\odot \approx B(5800K)$ ,

$$I = B(5800K)e^{-\tau_s} + B(4000K)\tau_s$$

In this case the contrast of the solar “cloud” will be reduced by the second term but in principle, if very fine structure absorbing clouds exist on the solar surface, then they will be visible against the solar disk. This is indeed observed (*e.g.* Sekse, Rouppe van der Voort, and De Pontieu, 2012; Lipartito *et al.*, 2014).

As a third example, we imagine observing strong lines (chromospheric lines) far above the solar limb. Source functions are determined by local conditions *and* the radiation within the emitting/absorbing atmospheric structure itself (this is also the case for the disk atmosphere, it’s just that here we imagine observing this plasma mostly tangentially not radially to the solar surface where the background intensity is zero). The opacities are also determined in this fashion, but there are classes of strong spectral lines for which the ambient radiation field is less important in the opacity than the source function. Consider the  $h$  and  $k$  lines of Mg II for example. The lower level populations of Mg II throughout the chromosphere are essentially decoupled from the source functions of these lines themselves, being simply proportional to the number density of  $\text{Mg}^+$ . This number density can be determined by local conditions. In this situation, very fine structure in “threads” or “blobs” will be resolved by the telescope independent of the mfp of photons, since the intensity is either

$$I = \int S d\tau_{LOS} \quad \text{optically thin}$$

or

$$I \approx S(\tau_{LOS} = 1) \quad \text{optically thick}$$

Again, either a ray intercepts some plasma - influencing  $\tau$  and  $S$  (which may itself be smeared), or it does not. Thus if the differences in  $\tau$  between rays are large then in both thick and thin cases the telescope should resolve these features.

This same optically thin argument applies to a fourth case, optically thin coronal lines, where we have seen structures down to  $0.3''$  scales when the photon mfps are almost infinite.

A fifth kind of example involves decoupling of source functions and optical depths via Doppler shifts. In the case of spectral lines, the source function has not just a  $\Lambda$  operator smoothing variations in  $S$  over depth, but also it has integral operators coupling different frequencies. We simply point out that the local mfp varies greatly in frequency so that relatively modest Doppler shifts can decouple the optical depth scale from the source function. Under such circumstances this decoupling can make the optical depths between adjacent rays through plasma moving with different Doppler velocities very different, analogous to the cloud cases discussed above but for a slightly different reason. Again such structure is observed (Judge, Reardon, and Cauzzi, 2012).

These examples reveal that one must carefully understand the nature of the source functions when observing below typical photon mean free paths.

## 5. Conclusions

The Sun itself sets fundamental limitations on the ultimate “resolution” that can be obtained, even in the photosphere where LTE is often assumed. On scales below photon mean free paths, in the presence of scattering in typical permitted photospheric lines, LTE breaks down since the source function appears to be in LTE only on larger physical scales where  $J$  can approach  $B$ . The decoupling of source function from local conditions produces smeared images which are qualitatively similar to those produced with a telescope PSF which has broad wings. We have tried to unify the literature by drawing attention to the different scattering parameters used by various workers and by using MTF and PSF characterizations of the atmosphere, following (Kneer, 1981). We have identified some simple scaling laws that might be useful when observing at and below the pressure scale height. On the basis of our study, we suggest that simultaneous imaging with both strongly and weakly scattering lines be conducted with high resolution telescopes. These might include several of the permitted Fe I lines and the two spin-forbidden Fe I lines at 524.7 and 525.0 nm.

The effects discussed are non-LTE effects of one particular kind, represented by equation (1). These are nLTE effects entering through the *source function*. Other multi-level effects include over-ionization of neutral species by non-LTE ionizing radiation, affecting primarily the *optical depth scale*, and the (implicit) influences of other bound-bound radiative transitions on the source function of a particular line. In principle, such effects should add to the smearing effects outlined here through the additional non-local processes involved.

**Acknowledgements** Philip Judge is very grateful to NAOJ for support of a Visiting Professorship there during July and August of 2012, where this work was begun.

## Appendix

### A. Mean free paths and scale heights

Photons emerging from an optically thick atmosphere arise mostly from regions centered around optical depth  $\tau = 1$ . As Landi Degl’Innocenti (2013) has pointed out, in stratified layers this has the curious property that *irrespective of the strength of the transition*, the photons emerge from a region with an intrinsic thickness of  $\approx 1$  pressure scale height, when the opacity is proportional to pressure. This scale represents a basic limit below which one cannot say with certainty that a certain photon arose from or “forms at” a specific height. This statement applies to all features formed in optically thick stratified layers, in particular throughout the photosphere and the subsonic (non-spicular) components of the chromosphere<sup>2</sup>.

We can show this result formally. Let  $z$  measure local height above some arbitrary point in the Sun, with the observer at  $\infty$ . The photosphere and low

---

<sup>2</sup>See appendix B.

chromosphere comprise a partially ionized stratified layer with  $T \approx 6000$  K, and a pressure scale height

$$H = - \left( \frac{d \ln p}{dz} \right)^{-1} = \frac{kT}{\mu m_H g} \approx 130 \text{ km.} \quad (13)$$

Across the solar photosphere-chromosphere, temperature changes by less than a factor of two whereas the pressure changes by orders of magnitude. Thus both gas density and pressure vary roughly as  $e^{-z/H}$ . Define the optical depth as usual,

$$\tau(z) = - \int_{\infty}^z k(s) ds \quad (14)$$

where  $k(s) = \lambda(s)^{-1}$  and  $\lambda(s)$  is the local mean free path of photons. We can also factor the opacity into  $k(s) = \kappa(s)\rho(s)$  where  $\kappa$  is the opacity in  $\text{cm}^2\text{g}^{-1}$ , often a slowly varying quantity, and  $\rho(s)$  the mass density in  $\text{g cm}^{-3}$ .

Define the region from which most photons emerge as between, say,  $\tau = 1/e$  and  $\tau = e$ . The geometrical thickness of this region is  $\Delta = z_1 - z_2$  where

$$e^{-1} = - \int_{\infty}^{z_1} k(s) ds, \quad e^{+1} = - \int_{\infty}^{z_2} k(s) ds. \quad (15)$$

In the photosphere, opacity is dominated by the minority species  $\text{H}^-$  (*e.g.* Allen, 1973). In this case  $\kappa \propto n_e$  where  $n_e$  is the electron density, and in this case,  $n_e \propto \rho$  since electrons come from singly ionized Fe, Si... (There is also a temperature dependence through the Saha  $\text{H}$ ,  $e$  and  $\text{H}^-$  equilibrium which is important in deep photospheric layers, ignored here for simplicity). Above the photosphere,  $\kappa$  is dominated by lines and continua of neutrals and singly ionized ions ( $\text{H}^-$  being negligible at smaller densities), and the opacity  $\kappa(s) \approx \text{constant}$  (*e.g.* Vernazza, Avrett, and Loeser, 1981). We can write, roughly,

$$\kappa(s) = \kappa(0) \left( \frac{\rho(s)}{\rho(0)} \right)^m$$

where  $m = 1$  (photosphere:  $\text{H}^-$ ) and  $m = 0$  (chromosphere). So for a simply stratified atmosphere we have

$$k(s) = k(0)e^{-(m+1)s/H}. \quad (16)$$

Combining with eq. (15) we have

$$e^{-1} = \frac{k(0)H}{m+1} e^{-z_1(m+1)/H}, \quad e^{+1} = \frac{k(0)H}{m+1} e^{-z_2(m+1)/H}. \quad (17)$$

The thickness of the region emitting most observed photons (*i.e.* those actually emerging from the atmosphere) is simply

$$\Delta = (z_1 - z_2) = 2H/(m+1). \quad (18)$$

Now, the mean free path of a photon where  $\tau = 1$  is  $1/k(\tau = 1)$  must be  $\approx \Delta$ : if it were larger (say  $10\Delta$ ) then this would mean that photons 10x deeper would escape, contrary to our assertion that they escape from  $\tau = 1$ ; if smaller, the photons would not escape, thus

$$\lambda \approx \Delta = 2H/(m + 1). \quad (19)$$

(The factor of two arises simply because of our adoption of brightness factors  $e$  and  $1/e$ ). The photon path length is of the same order as the pressure and density scale height in the photosphere ( $m = 1$ ) and lower chromosphere ( $m = 0$ ).

## B. Surely the chromosphere is not hydrostatic?

When fluid motions are subsonic, the atmosphere cannot be far from a hydrostatic state. This is because sound/ magnetosonic waves propagate changes in pressure to make the atmosphere approach a balance between pressure gradients and gravity. Much attention has been drawn to chromospheric features with highly supersonic motions. The classic semi-empirical, hydrostatic models of VAL (*e.g.* Vernazza, Avrett, and Loeser, 1981) have been much maligned, the chromosphere at the limb appears at a first glance to be extended much beyond the 1.5 Mm thickness of the model. So what is going on here?

Those features moving supersonically include spicules and rapidly moving features seen on the solar disk. We can estimate what fraction of the Sun is covered at any given time by these rapid events using numbers recently published by Sekse and colleagues (Sekse, Rouppe van der Voort, and De Pontieu, 2012), revising earlier estimates by Judge and Carlsson (2010). The former authors find up to  $2 \times 10^5$  of these features on the Sun at any given time. Each is typically  $\ell = 2.5$  Mm long and say at most  $w = 0.2$  Mm across. Thus the area covered by these features is  $< w\ell = 10^5$  Mm<sup>2</sup>, of a total solar surface area of  $6 \times 10^6$  Mm<sup>2</sup>. Thus by these data, at most just 1.7% of the Sun's chromosphere has supersonic motions associated with it. This appears broadly consistent with the images shown by these authors, only a small fraction of the solar surface shows these features.

However it has been claimed by some that there is “no chromosphere” when there is no clear fibril structure. Given that many fibrils are supersonic, the claim might be extended to mean that there is no hydrostatic layer. It is difficult to assess what this claim might mean since the Sun cannot go immediately from photospheric pressures to coronal pressures with no intervening plasma pressure or magnetic stress- they differ by five (!) orders of magnitude. While claims and opinions may change, data do not. It is clear, and has been for some time, that if one observes narrow chromospheric line profiles on the solar disk, features with supersonic motions are quite rare. Using observations of C I emission emission lines from HRTS, for example, Dere, Bartoe, and Brueckner (1983) found that supersonic chromospheric “jets” are born at a rate of some  $3 \times 10^{-4}$  Mm<sup>-2</sup> s<sup>-1</sup> with a lifetime of 40s or so, and each has an area of some 1 Mm<sup>2</sup>. Using these figures we see that they cover just 1% or so of the total area of the chromosphere.

Therefore, we must recognize that the bulk of the chromosphere is approximately stratified in hydrostatic equilibrium. This is also consistent with early analyses of the solar flash spectrum (Athay, 1976) and the existence of 3-5 min oscillations throughout much of the chromosphere requires a hydrostatic stratification. As far as the chromosphere is concerned, the supersonic features are interesting but fill only a tiny fraction of the entire chromosphere.

## References

- Allen, C.W.: 1973, *Astrophysical quantities*, Athlone Press, Univ. London.
- Athay, R.G.: 1976, *The solar chromosphere and corona: Quiet sun*, Reidel, Dordrecht.
- Avrett, E.H., Loeser, R.: 1971, Radiative transfer in two-component stellar atmospheres. *J. Quant. Spectrosc. Radiat. Transfer* **11**, 559–571.
- Bruls, J.H.M.J.: 1993, The formation of helioseismology lines. iv. the ni i 676.8 nm intercombination line. *Astron. Astrophys.* **269**, 509–517.
- Bruls, J.H.M.J., Von der Lühe, O.: 2001, Photospheric fine structure: An observational challenge. An analysis of radiative transfer effects on the visibility of small-scale structures. *Astron. Astrophys.* **366**, 281–293.
- Cauzzi, G., Reardon, K.P., Uitenbroek, H., Cavallini, F., Falchi, A., Falciani, R., Janssen, K., Rimmele, T., Vecchio, A., Wöger, F.: 2008, The solar chromosphere at high resolution with IBIS. I. New insights from the Ca II 854.2 nm line. *Astron. Astrophys.* **480**, 515–526.
- Dere, K.P., Bartoe, J.-D.F., Brueckner, G.E.: 1983, Chromospheric jets - Possible extreme-ultraviolet observations of spicules. *Astrophys. J.* **267**, L65–L68.
- Faurobert, M., Ricort, G., Aime, C.: 2013, Empirical determination of the temperature stratification in the photosphere of the quiet Sun. *Astron. Astrophys.* **554**, A116.
- Holzreuter, R., Solanki, S.K.: 2012, Three-dimensional non-LTE radiative transfer effects in Fe I lines. I. Flux sheet and flux tube geometries. *Astron. Astrophys.* **547**, A46.
- Holzreuter, R., Solanki, S.K.: 2013, Three-dimensional non-LTE radiative transfer effects in Fe I lines. II. Line formation in 3D radiation hydrodynamic simulations. *Astron. Astrophys.* **558**, A20.
- Judge, P.G., Carlsson, M.: 2010, On the Solar Chromosphere Observed at the limb with Hinode. *Astrophys. J.* **719**, 469–473.
- Judge, P.G., Reardon, K., Cauzzi, G.: 2012, Evidence for Sheet-like Elementary Structures in the Sun's Atmosphere? *Astrophys. J. Lett.* **755**, L11.
- Kiselman, D., Nordlund, A.: 1995, 3D non-LTE line formation in the solar photosphere and the solar oxygen abundance. *Astron. Astrophys.* **302**, 578.
- Kneer, F.: 1981, Multidimensional radiative transfer in stratified atmospheres. *Astron. Astrophys.* **93**, 387–394.
- Knoelker, M., Schuessler, M., Weisshaar, E.: 1988, Model calculations of magnetic flux tubes. III - Properties of solar magnetic elements. *Astron. Astrophys.* **194**, 257–267.
- Landi Degl'Innocenti, E.: 2013, Spectropolarimetry with new generation solar telescopes. *Memorie della Societa Astronomica Italiana* **84**, 391.
- Leenaarts, J., Carlsson, M., Rouppe van der Voort, L.: 2012, The Formation of the H $\alpha$  Line in the Solar Chromosphere. *Astrophys. J.* **749**, 136.
- Leenaarts, J., Rutten, R.J., Reardon, K., Carlsson, M., Hansteen, V.: 2010, The Quiet Solar Atmosphere Observed and Simulated in Na I D<sub>1</sub>. *Astrophys. J.* **709**, 1362–1373.
- Linsky, J.L., Ayres, T.R.: 1978, *Astrophys. J.* **220**, 619.
- Lipartito, I., Judge, P., Reardon, K., Cauzzi, G.: 2014, The solar chromosphere observed at 1 hz and 0."2 resolution. *ArXiv e-prints*.
- Lites, B.W.: 1973, The Solar Neutral Iron Spectrum. II: Profile Synthesis of Representative Fe I Fraunhofer Lines. *Solar Phys.* **32**, 283–306.
- Mihalas, D.: 1978, *Stellar atmospheres*, W. H. Freeman and Co., San Francisco (second edition).
- Norton, A.A., Graham, J.P., Ulrich, R.K., Schou, J., Tomczyk, S., Liu, Y., Lites, B.W., López Ariste, A., Bush, R.I., Socas-Navarro, H., Scherrer, P.H.: 2006, Spectral Line Selection for HMI: A Comparison of Fe I 6173 Å and Ni I 6768 Å. *Solar Phys.* **239**, 69–91.
- Owocik, S.P., Auer, L.H.: 1980, Two-dimensional radiative transfer. ii. the wings of ca k and mg k. *Astrophys. J.* **241**, 448–458.

- Rempel, M.: 2014, Numerical Simulations of Quiet Sun Magnetism: On the Contribution from a Small-scale Dynamo. *Astrophys. J.* **789**, 132.
- Rybicki, G.B., Hummer, D.G.: 1991, An accelerated lambda iteration method for multilevel radiative transfer i. non-overlapping lines with background continuum. *Astron. Astrophys.* **245**, 171–181.
- Scharmer, G.B., Carlsson, M.: 1985, A new approach to multi-level non-lte radiative transfer problems. *J. Comput. Phys.* **59**, 56–80.
- Seaton, M.J.: 1962, The theory of excitation and ionization by electron impact. In: Bates, D.R. (ed.) *Atomic and Molecular Processes*, Academic Press, New York, 11.
- Sekse, D.H., Rouppe van der Voort, L., De Pontieu, B.: 2012, Statistical Properties of the Disk Counterparts of Type II Spicules from Simultaneous Observations of Rapid Blueshifted Excursions in Ca II 8542 and H $\alpha$ . *Astrophys. J.* **752**, 108.
- Socas-Navarro, H.: 2005, The Three-dimensional Structure of a Sunspot Magnetic Field. *Astrophys. J. Lett.* **631**, L167–L170.
- Stenholm, L.G., Stenflo, J.O.: 1977, Multi-dimensional non-LTE radiative transfer in magnetic fluxtubes on the sun. *Astron. Astrophys.* **58**, 273–280.
- Stenholm, L.G., Stenflo, J.O.: 1978, Multi-dimensional Non-LTE Transfer of Polarized Radiation in Magnetic Fluxtubes. *Astron. Astrophys.* **67**, 33.
- Uitenbroek, H.: 2000, The CO Fundamental Vibration-Rotation Lines in the Solar Spectrum. I. Imaging Spectroscopy and Multidimensional LTE Modeling. *Astrophys. J.* **531**, 571–584.
- Van Regemorter, H.: 1962, Rate of collisional excitation in stellar atmospheres. *Astrophys. J.* **136**, 906.
- Vernazza, J.E., Avrett, E.H., Loeser, R.: 1981, Structure of the solar chromosphere. iii - models of the euv brightness components of the quiet-sun. *Astrophys. J. Suppl. Ser.* **45**, 635.